ORIGINAL RESEARCH **Open access**

A Robust Crop Row Detection Method Based on Regional Feature Clustering in Field Environments

Kenji Tanaka[1*], Yui Kobayashi[1]

Abstract

To overcome the challenges of low precision and high computational time in conventional machine vision-based crop row detection—arising from differences in crop types, growth conditions, and varying numbers of crop rows—this paper presents a centerline extraction technique utilizing regional feature point clustering. First, vegetation is segmented from the background using the 2G-R-B feature factor and an optimized adaptive thresholding approach. Next, a closing-then-opening morphological procedure is executed to suppress weeds and crop edges, minimizing disturbances. Harris corner detection is then employed to identify crop feature points, which are subsequently grouped through the DBSCAN algorithm, with each crop row labeled in a distinct color. Following this, the image is divided horizontally into several strips, and the center point of every feature point cluster within each strip is computed. Ultimately, the least-squares technique is applied to fit midpoints for each row, producing the crop row centerline. Experimental evaluations reveal that this method delivers high-accuracy centerline extraction across four crop varieties: sweet potato, mint, corn, and peanut. The average row recognition rate reached 98.33%, with a mean angular error of 0.95°. Furthermore, the mean processing time per image was 136.14 ms, yielding an average time saving of 69.22 ms compared to the traditional Hough transform and 87.33 ms compared to the skeleton extraction approach. Overall, the proposed method provides a more resilient alternative for crop rows under diverse field conditions.

Keywords Image processing, Computer vision, Segmentation, DBSCAN clustering, Least squares method, Crop row extraction

*Correspondence:
Kenji Tanaka
tanaka.kenji@mail.ecc.u-tokyo.ac.jp
[1] Department of Artificial Intelligence for Rice Growth Modeling, Graduate School of Agricultural and Life Sciences, University of Tokyo, Tokyo, Japan

Introduction

The rapid progress of smart and precision agriculture in recent years has made autonomous navigation for agricultural machinery a critical technology in the farming sector, with widespread use for tasks such as plowing, weeding, planting, spraying, fertilizing, and harvesting [1-3]. Its significance lies in reducing input costs, boosting working efficiency and accuracy, and elevating both the economic returns and societal contributions of agricultural operations. Currently, navigation relies chiefly on satellite-based systems and machine vision [4]. Satellite navigation typically leverages the Global Navigation Satellite System (GNSS) to provide centimeter-level accuracy; however, it suffers from signal blockage by tree canopies and an inability to interpret specific crop-row characteristics. In contrast, machine vision can capture real-time relative positioning data of crop rows while monitoring current crop development and the surrounding field environment [5, 6]. Due to its low cost, it is widely adopted for detecting and identifying live crops [7, 8], weeds [9, 10], and crop rows [11, 12].

This is an open access article distributed under the terms of the Creative Commons Attribution-NonCommercial-ShareAlike 4.0 International License (CC BY-NC-SA 4.0), which permits non-commercial use, distribution, reproduction, and adaptation in any medium or format, provided that appropriate credit is given to the original author(s) and source, a link to the license is provided, and any changes made are indicated. Adapted material must be distributed under the same license.

© 2022 The Author(s). | Published by Agro Intelligence Research Press

Winterhalter *et al.* [13] devised a small-scale crop-row detection method based on Hough transform patterns, suitable for recognizing rows throughout the growth period and for calculating the angular deviation and displacement of agricultural robots. García-Santillán *et al.* [14] isolated green pixels based on color attributes and used a linear regression model for row extraction, thereby overcoming the drawbacks of the classical Hough transform. However, this technique demands advanced information about inter-row spacing. Jiang *et al.* [15] scanned binary images using a sliding rectangular window to obtain wheat-row feature points and applied the Hough transform for detection, achieving over 90% accuracy. Zhang *et al.* [16] described a row extraction methodology based on position clustering and the shortest-path algorithm, which proved effective for early-stage maize rows with weed presence. Diao *et al.* [17] formulated a corn row recognition framework based on ST-YOLOv8s and assembled a dataset spanning multiple growth phases. Through refinements in detection and segmentation, row line detection accuracy improved by 5.99%–17.38% at the segment level. Vidović *et al.* [18] presented a scheme that uses dynamic programming to search for optimal points across the global dataset, accurately detecting both linear and curved rows; however, its scope is confined to scenarios with a known count of 2–3 rows, making it unsuitable for unknown or numerous rows. Deep learning techniques have also recently been harnessed for crop row extraction. Diao *et al.* [19] proposed a navigation line extraction algorithm for corn-spraying robots using an improved YOLOv8s, where ASPPF-YOLOv8s identifies plant cores, and the least-squares method fits the centerline. Pang *et al.* [20] introduced the Maximum Area Mask Score Region Neural Network to extract maize seedling rows from aerial imagery.

To precisely identify the centerline of crop rows, a region-based feature-point clustering approach is introduced.

· The 2G-R-B feature factor, together with an optimized adaptive threshold segmentation scheme, separates the crops from the background.

· Morphological processing involving closing followed by opening is performed to eliminate weeds and smooth crop boundaries. The Harris corner detector then extracts crop feature points, which are grouped using the DBSCAN algorithm, and each cluster is assigned a unique color to support identification of crop rows. The image is split horizontally into multiple strips, and within each strip, the midpoint of each feature point cluster is determined. The assigned cluster color is transferred to its respective midpoint, thereby discarding irrelevant features and reducing computational load.

· Midpoints are matched by color label, with identically colored points treated as members of the same crop column. A least-squares linear regression is subsequently performed for each color group to derive the crop row centerlines.

Image Preprocessing

Grayscale conversion of farmland images

The conversion of color imagery to grayscale is a vital preparatory stage in the image segmentation pipeline [21], as the fidelity of this transformation directly influences the accuracy with which navigation lines can later be extracted. Vegetation within crop row photographs is largely green in appearance, and any perceivable color emerges from the additive mixing of red, green, and blue—the three fundamental chromatic components. Taking a point whose color is specified as RGB(r,g,b), a computational rule is executed to collapse its three channel values into a single intensity measure, termed gray, which subsequently generates a new color definition RGB(gray, gray, gray). Here, the initial R, G, and B channels are uniformly overwritten by the gray intensity, thereby yielding the grayscale equivalent of that spatial point [22]. Within the RGB color model, the G channel of unprocessed crop row images consistently registers higher than both the R and B channels [23]. Capitalizing on this tendency, deliberately emphasizing the G contribution throughout the grayscale conversion helps discriminate living plant material from the underlying soil matrix. The Excess Green (EXG) grayscale formulation possesses the capacity to attenuate background artifacts such as desiccated grass and exposed earth **(Eq.1)**; however, it does not always succeed in making crop features sufficiently prominent. The present work refines the EXG factor. Recognizing that soil exhibits a comparatively elevated R channel proportion, our method

© 2022 The Author(s). | Published by Agro Intelligence Research Press

enhances the G channel while simultaneously curbing the R channel, thereby cleanly separating green vegetation from the soil substrate. Concurrently, the expression 2G(x,y)−B(x,y) is used to derive grayscale intensities, thereby helping smooth out grayscale inconsistencies across different regions of a single plant. The complete formula is stated as **Eq. 2**.

$$\text{gray}(x,y) = \begin{cases} 2G(x,y) - R(x,y) - B(x,y) & \text{else} \\ 255 & 2G - R - B > 255 \\ 0 & 2G - R - B < 0 \end{cases},$$

(1)

$$\text{gray}(x,y) = \begin{cases} 2G(x,y) - B(x,y) & G > R \text{ or } G > B \\ 0 & \text{else} \end{cases},$$

(2)

Where R, G, and B correspond respectively to the red, green, and blue channels of an RGB image. The term gray(x,y) denotes the grayscale factor. Subsequently, the crop row photograph is processed using the 2G-R-B algorithm, and the resulting visual output is shown in **Figure 1**.



Figure 1. Grayscale processing of images.

© 2022 The Author(s). | Published by Agro Intelligence Research Press

Image segmentation and morphological processing

Threshold-based segmentation is applied to the grayscale crop row image to produce a binary representation, thereby achieving a clean partition between foreground targets and the background [24]. The threshold value must be chosen to minimize the probability of misclassification [25]. The present study employs optimal adaptive thresholding for binarization. This technique operates by modeling the image's histogram as a composite of probability density functions from two or more normal distributions, and setting the segmentation threshold at the grayscale level corresponding to the lowest probability point between the distributions' peaks. Proceeding in this fashion drives the segmentation error probability toward its minimum. The procedure requires separate computation of the mean grayscale intensities for the background and foreground objects, from which the separating threshold T(i+1) is derived. Convergence to the optimal threshold is indicated when two successive iterations produce identical threshold values [26]. Should they differ, the means are recomputed, and the iterative cycle continues. The mathematical formulation appears in **Eqs. 3-5**.

$$\mu_B = \frac{\sum_{(i,j)\in \text{background}} f(i,j)}{\#\text{background_pixels}}, \quad (3)$$

$$\mu_O = \frac{\sum_{(i,j)\in \text{object}} f(i,j)}{\#\text{object_pixels}}, \quad (4)$$

$$T^{(i+1)} = \frac{\mu_B + \mu_O}{2}. \quad (5)$$

Within these equations, f(i,j) represents the intensity of a given pixel; #background_pixels indicates the total count of background-classified pixels; and #object_pixels indicates the total count of object-classified pixels. Following binarization, to neutralize the confounding effects of field weeds and non-uniform lighting conditions on crop extraction, this paper applies a sequence of morphological closing followed by opening to denoise and fill gaps in the binary image. The closing operation is adept at erasing small-scale noise artifacts, yet it can inadvertently create sizeable hollow regions within crop bodies [27]. The subsequent opening operation then serves to backfill those hollows, as shown in the morphological processing outcome in **Figure 2**.

© 2022 The Author(s). | Published by Agro Intelligence Research Press

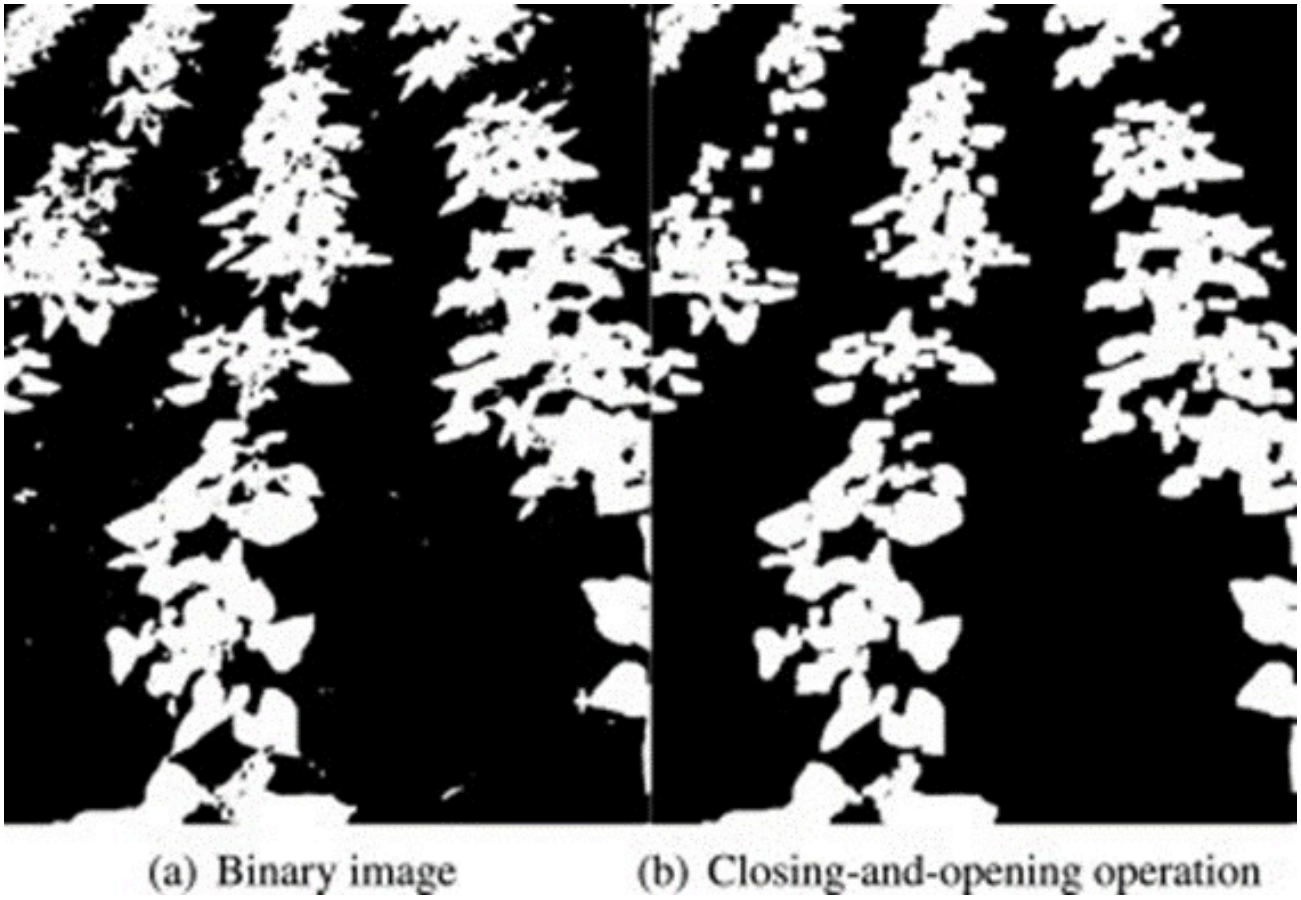

Figure 2. Binaryzation and mathematical morphology.

The Acquisition of Crop Row Feature Points

Given that the vast majority of crops are established either by row-based sowing or transplanting, crop rows observed over moderate distances can reasonably be approximated as linear structures [28]. The theoretical row line traverses each plant at its root-stem junction [29]. In practice, however, this junction is obscured by overhanging leaves, so only feature points collected from the visible foliage can be used. This paper introduces an extraction methodology grounded in region-based feature-point clustering to derive crop-row characteristics. As shown in **Figure 3a**, Harris corner detection is used to locate and extract salient feature points from crop images; these points predominantly coincide with leaf edges and corners, which serve as useful indicators of crop morphology and spatial arrangement. As shown in **Figure 3b**, the DBSCAN clustering algorithm is subsequently applied to partition the extracted feature points, column by column, into distinct groupings that mirror the spatial spread of feature points across the different planting rows. Afterwards, the full image is subdivided into a series of horizontal strips, each of height h, and within each strip, the midpoint of each feature point cluster is computed. These midpoints serve as condensed representations of the columns within each horizontal band, providing essential clues about the structural layout of the crop rows.

© 2022 The Author(s). | Published by Agro Intelligence Research Press

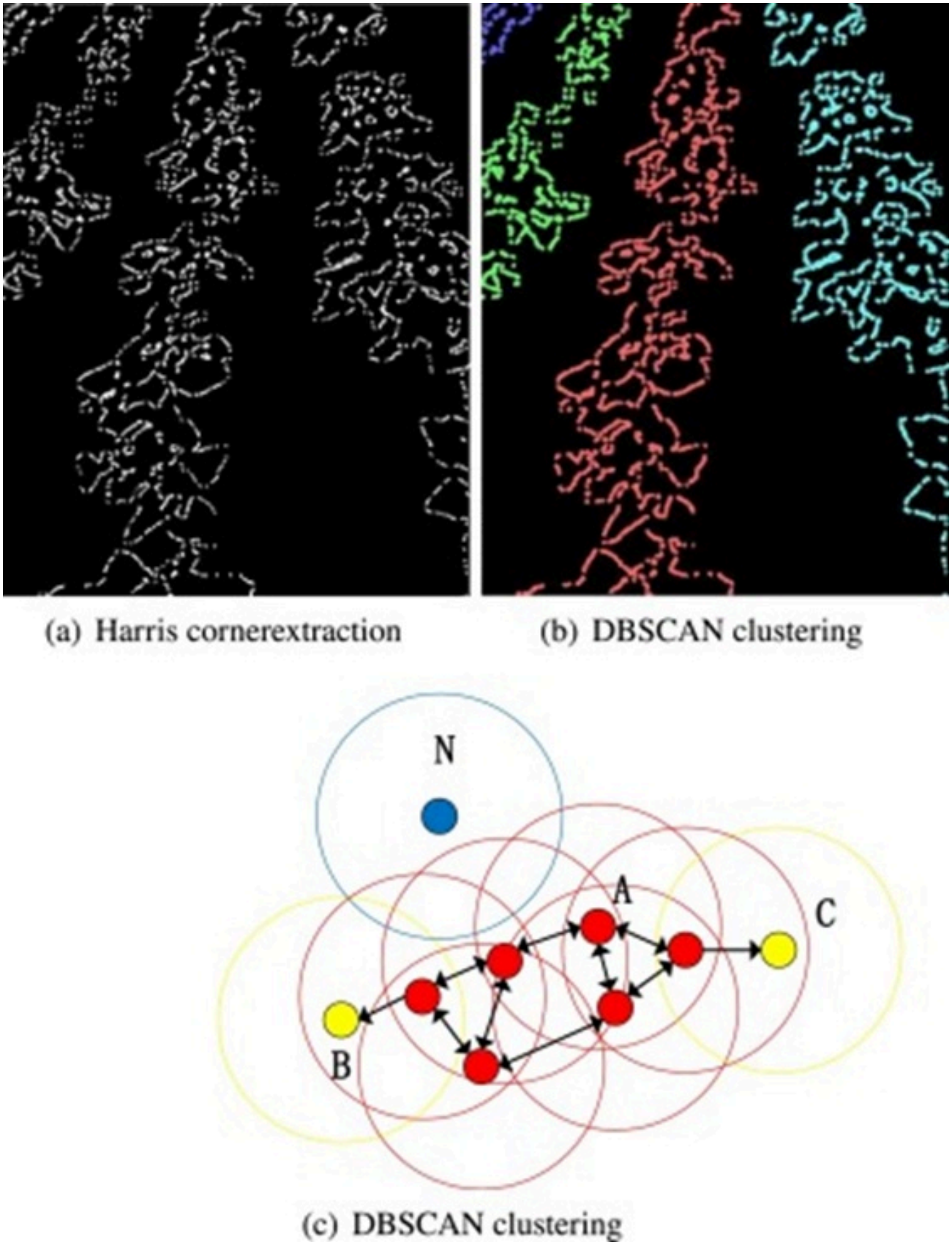

Figure 3. Feature point extraction and clustering.

© 2022 The Author(s). | Published by Agro Intelligence Research Press

DBSCAN (Density-Based Spatial Clustering of Applications with Noise) is a non-parametric clustering methodology that dispenses with any requirement to stipulate the number of clusters beforehand [30, 31]. Its fundamental purpose is to uncover regions of sufficiently high point density within the image, thereby allocating feature points into separate clusters while concurrently identifying outliers. As schematically represented in **Figure 3c**, for any given feature point, if the zone within a distance threshold epsilon around it contains a count of other feature points equal to or exceeding a specified minimum (min_sample), that point is designated a core object. All points residing within this surrounding neighborhood are termed directly density-reachable from it. When a feature point falls within the neighborhood of another core object, and a connection exists, it likewise qualifies as directly density-reachable, thereby implying eligibility for membership in the same cluster. In cases where a sequence of feature points can be traced such that each successive point is directly density-reachable from the previous one, the two endpoints of this chain are said to be density-reachable, a property that sometimes enables a cluster to stretch across relatively sparse intervening regions. Any feature point that qualifies neither as a core object nor as density-reachable is labeled as a noise point and is not assigned to any cluster. Each crop row is treated as a single cluster of feature points and visually coded with a unique color.

Owing to the considerable variation in plant stature and in-row spacing across different crop species, the two pivotal DBSCAN parameters—namely epsilon (the radius defining a point's neighborhood) and min_samples (the minimum number of neighboring points needed to establish a core point)—must be calibrated separately for each crop context. To begin with, epsilon dictates how far a point's influence extends. Because plant dimensions vary from one crop to another, an appropriately sized neighborhood radius must be selected for each crop. As shown in **Figures 4a and 4b**, setting epsilon too small may prevent points that genuinely belong together from being recognized as a single entity, while setting it too large risks merging points that actually belong to separate clusters. Secondly, the min_samples parameter sets the threshold for core point status. Planting density varies among crops; densely sown crops call for a higher min_samples figure, whereas sparsely sown crops demand a lower one to keep core point designations sensible. In short, when putting DBSCAN to work, individually tailoring epsilon and min_samples for each crop type is a crucial step toward improving both the quality and correctness of the clustering outcomes. After numerous rounds of experimental tuning, the finalized threshold configurations for the four crop clustering routines are presented in **Table 1**. The influence of different epsilon settings on clustering performance is shown in **Figure 5**, where the horizontal axis tracks epsilon values and the vertical axis records the row recognition rate, substantiating the optimality of the parameters listed in the table. Because adjustments within the min_samples range produce only a weak marginal impact on the row recognition rate (changes in core point density mainly tweak the precision of noise rejection rather than the grouping of crop rows themselves), the incremental benefit of additional experimentation is limited. It could shift attention away from the more critical epsilon parameter. For this reason, dedicated ablation experiments are not deemed necessary.

© 2022 The Author(s). | Published by Agro Intelligence Research Press

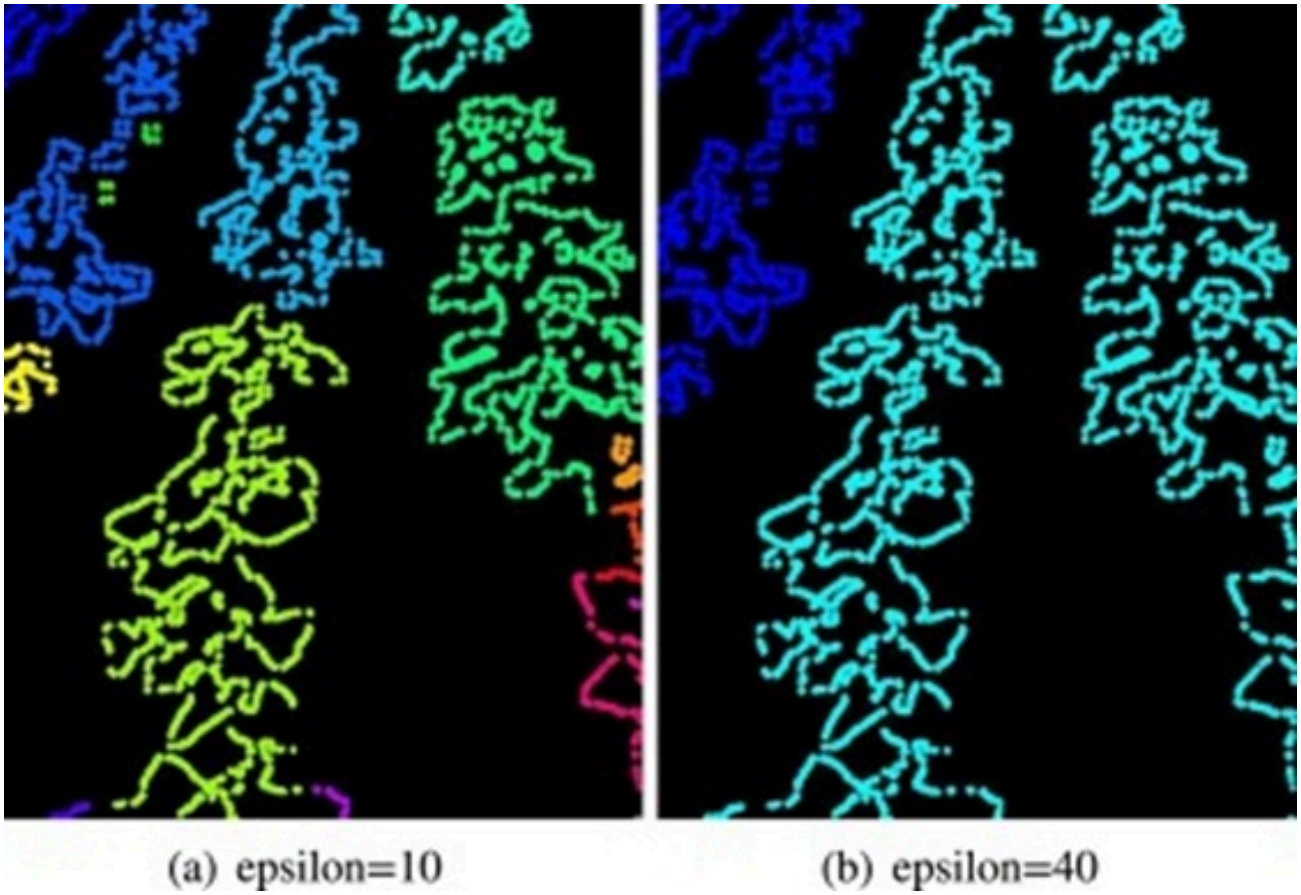

Figure 4. Clustering Results with Different Thresholds.

Table 1. Threshold settings for four crop clustering algorithms.

Crops	*min_sample*	*epsilon*
Sweet potato	5	25
Mint	5	28
Corn	20	36
Peanut	20	45

© 2022 The Author(s). | Published by Agro Intelligence Research Press

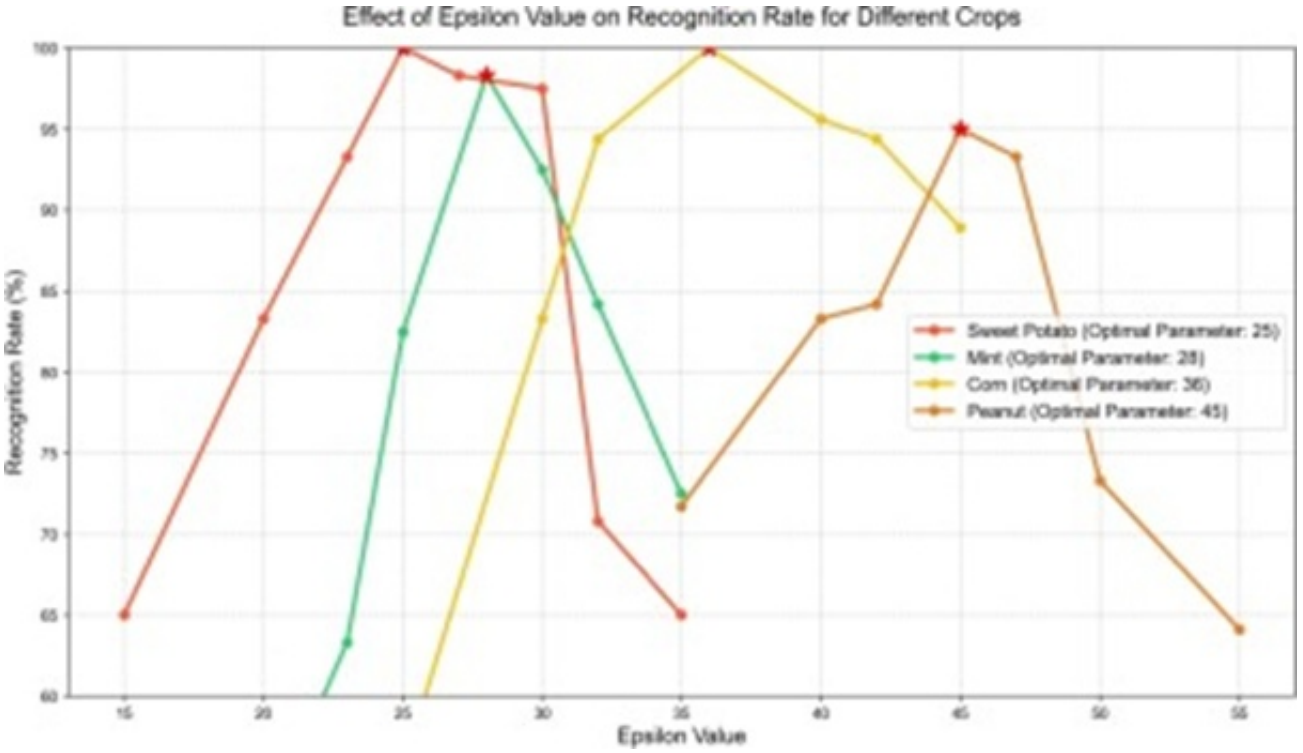

Figure 5. Effect of epsilon on recognition rate for different crops.

In the present work, feature points across crop images were first grouped using the DBSCAN algorithm, and the resulting cluster maps were subsequently split into multiple horizontal strips. The image width was set to W, and its height to H. To enable a more fine-grained examination, the image was carved along its vertical extent into several horizontal slices, each of height h and dimensions W×h, such that the total number of strips n equals H/h.

Through iterative testing and systematic parameter optimization, the ideal strip height h was determined. Using sweet potato centerline extraction as a representative case, the collected experimental measurements indicate: when h = 20, the angular deviation comes to 0.71° with a processing duration of 100.79 ms; when h = 40, the angular deviation is 0.76° while the processing duration drops to 91.83 ms; when h = 60, the angular deviation expands to 1.56° and the processing duration falls to 89.81 ms.

Evaluating the trade-off from the twin perspectives of accuracy and runtime efficiency reveals the following: relative to h = 40, the h = 20 configuration shaves 0.05° off the angular error but at the cost of an extra 8.96 ms of processing time; meanwhile, moving to h = 60 saves 2.02 ms of processing time but introduces a sharp 0.8° worsening in angular error. Given that visual navigation line extraction imposes stringent requirements on both angular fidelity and computational speed. To secure the most favorable equilibrium between these competing demands, h = 40 emerges as the optimal parameter choice following a comprehensive appraisal of all relevant performance indicators.

Thereafter, each horizontal strip was processed in sequential order. For any given strip, an initial check determined whether any feature points were located within it. If points were detected, their color identifiers were then recognized. The count of distinct color identifiers present corresponds directly to the number of separate crop-feature-point cluster columns intersecting that strip. Next, to capture a single representative location for each cluster, a midpoint calculation was performed: within each horizontal strip, the point at the cluster's central spatial position was selected and assigned the cluster's color label. The particulars of these midpoints—position coordinates together with their color tags—were appended to a list designated midpoints_list to support downstream analysis and feature extraction. The procedure for harvesting midpoints across the horizontal strips is diagrammed in **Figure 6**. If a particular horizontal strip contained no

© 2022 The Author(s). | Published by Agro Intelligence Research Press

feature points, that strip was skipped, and the scan proceeded directly to the following strip. The rationale for this step is to gather compact yet representative signatures of the previously clustered feature point groups within each horizontal band, thereby facilitating a richer, more comprehensive characterization of the crop image content. Through this approach, crop feature data can be captured and analyzed with greater fidelity. The visual result of the midpoint extraction process is shown in **Figure 7**.

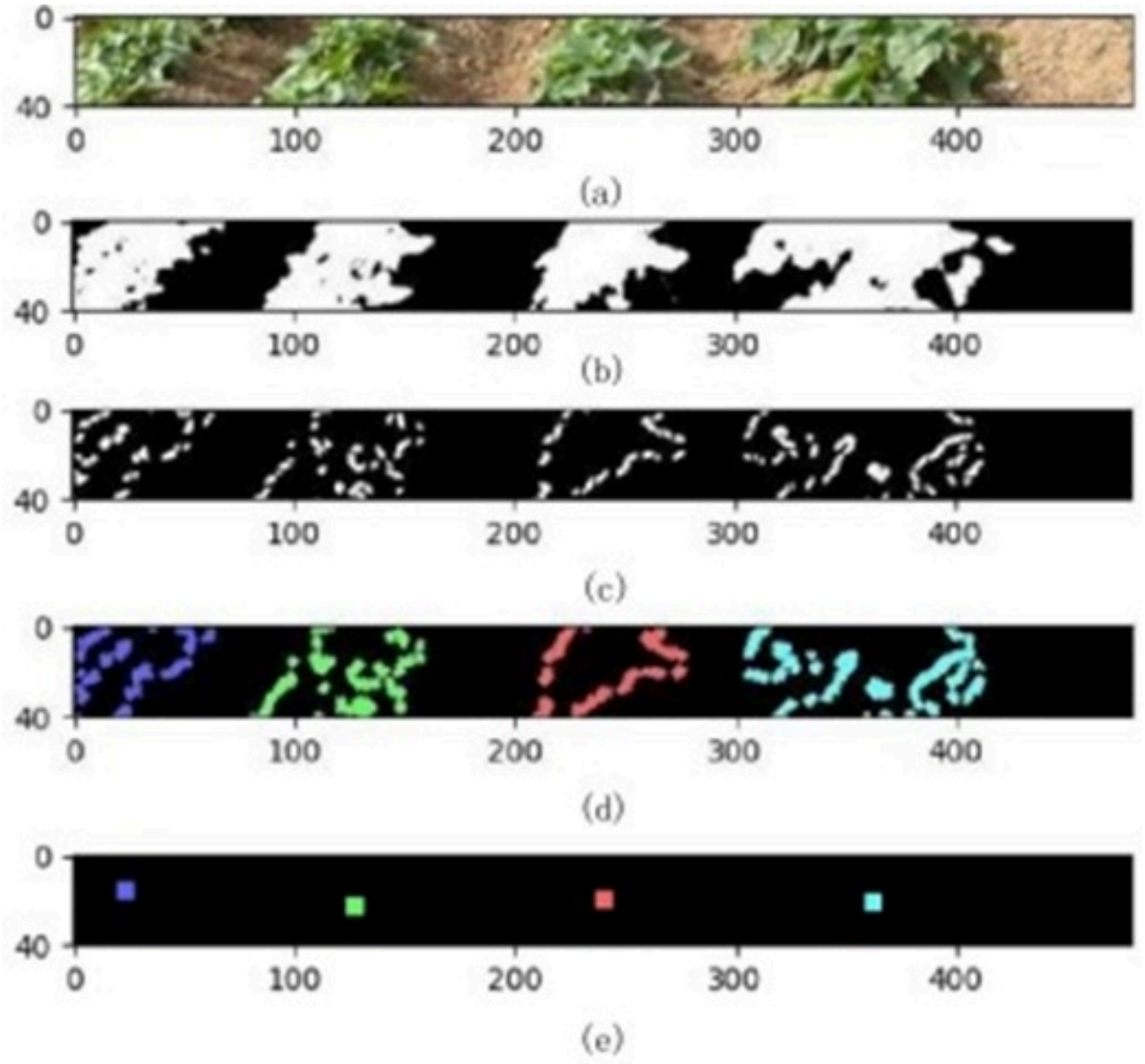

Note: Images 5a-5e describe the process of obtaining midpoints for each horizontal strip in image segmentation when h = 40.

Figure 6. Method for obtaining midpoints.

© 2022 The Author(s). | Published by Agro Intelligence Research Press

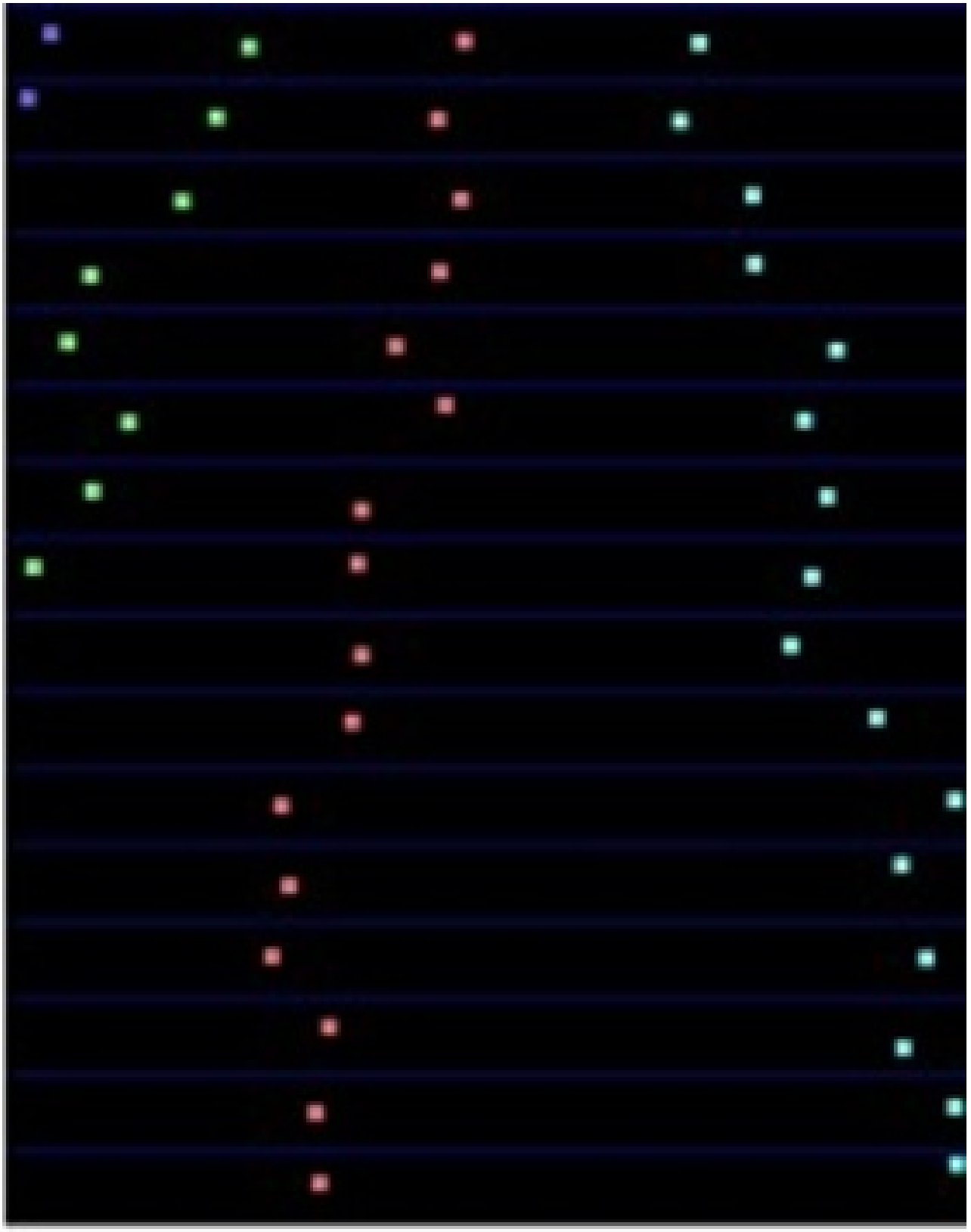

Note: Horizontal strips are divided

© 2022 The Author(s). | Published by Agro Intelligence Research Press

by blue line.

Crop Row Fitting

Two well-established techniques for line fitting are linear regression and the Hough transform. Among mathematical optimization tools, the Least Squares Method is widely used, as it identifies a parameter combination that minimizes the sum of squared residuals between an assumed model and empirical observations. Although linear models are most frequently applied within this framework, the method does not preclude other model formulations. For a supplied set of data coordinates (xi,yi) and the corresponding model-generated estimates yˆi, each residual is computed as yi−yˆi. The penalty function is constructed from the squared residuals, detailed in **Eq. 6**.

$$LOSS = \sum_{i=1}^{n} (y_i - \hat{y}_i)^2. \quad (6)$$

By taking the derivative of this penalty function and forcing it to zero, one arrives at the parameter values that produce the minimal loss. In a linear regression context, the sought parameters are typically the slope m and the vertical intercept b. Working from the collected data and the specified model structure, the optimal parameter estimates are derived to minimize the penalty function. When the task involves fitting straight lines to multiple crop rows simultaneously via least squares, the midpoints for each row must first be sorted into their respective groups. Then, an independent line-fitting computation is performed on the midpoint assembly for each row. Midpoints stemming from a single row are marked with a single shared color and stored in the list midpoints_list. By filtering out points with matching colors and collecting them into grouped_midpoints, one can subsequently perform individual fits for each color-coded set. This row-by-row treatment ensures that the distinctive layout of each crop row is properly accounted for, resulting in more faithful linear representations. The final fitted outputs are presented in **Figure 8**.

© 2022 The Author(s). | Published by Agro Intelligence Research Press



Figure 8. Least squares fitting results.

© 2022 The Author(s). | Published by Agro Intelligence Research Press

Accordingly, the overall pipeline of the proposed centerline extraction methodology, premised on regional feature point clustering, is outlined in **Figure 9**.

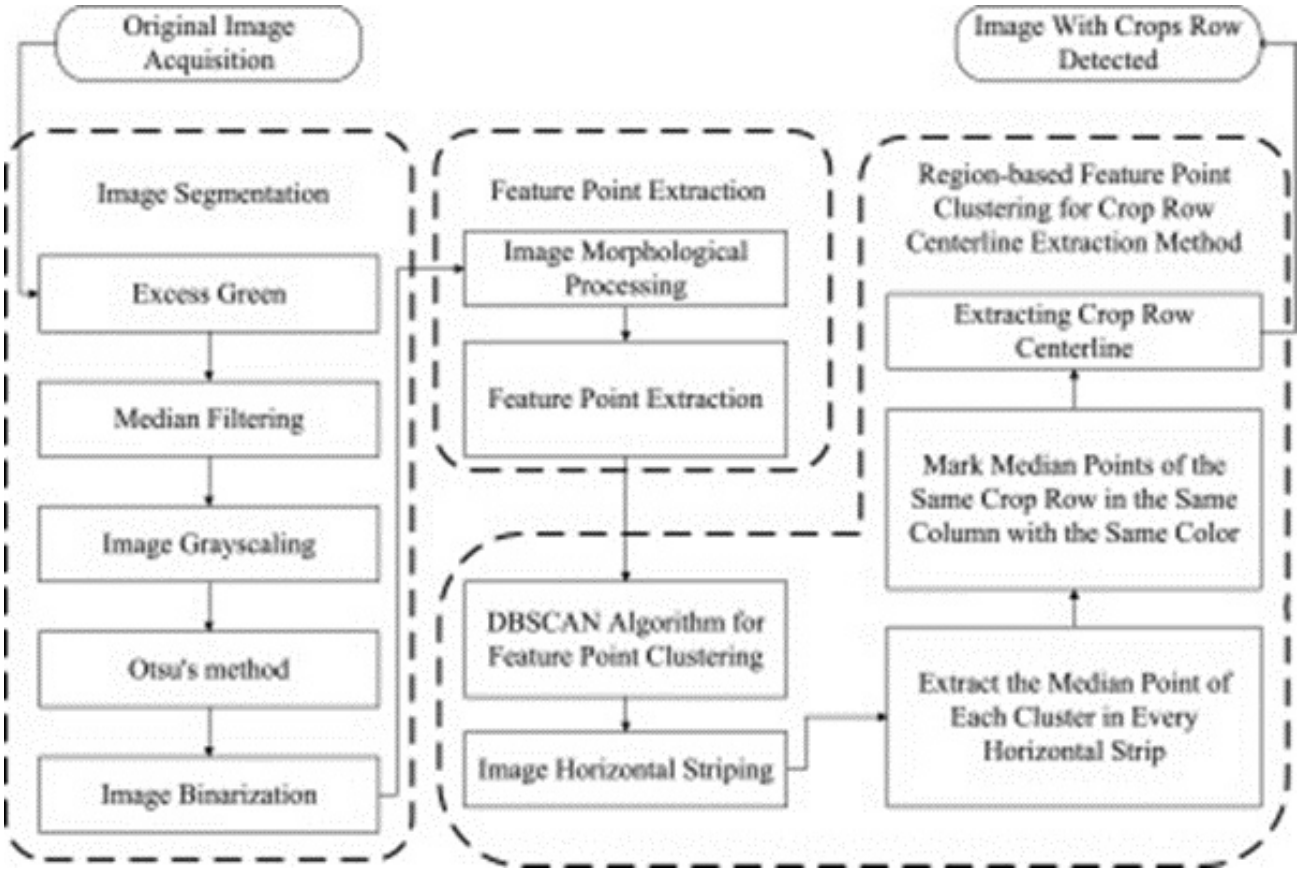

Figure 9. Flow chart of navigation path detection.

Experiment and Result Analysis

Experimental materials and preparation

To substantiate the real-time capability and correctness of the navigation line extraction scheme introduced here for robotic guidance, a four-wheel-drive agricultural robot is utilized as the experimental verification platform. To safeguard the onboard control computer and associated control hardware, the robot predominantly traverses flat ground, limiting ramp gradients to no more than 20 degrees. Exceeding this inclination may lead to a vehicle rollover. The core dimensional and performance parameters of the agricultural robot chassis are listed in **Table 2**.

Table 2. Basic parameters of the agricultural robot chassis.

Parameter	Specification/Performance
Rated Voltage (V)	24
Rated Current (A)	10
Rated Power (W)	100 W

© 2022 The Author(s). | Published by Agro Intelligence Research Press

No-Load Speed (rpm)	3000 rpm
Gear Reduction Ratio	27:1
Weight (kg)	26
Operating temperature range (°C)	-10–50
Maximum load capacity (kg)	5
Encoder resolution	500

Results and analysis

The side-by-side extraction outputs produced by our method, the Hough transform technique, and the skeleton extraction approach across four crop species are displayed in **Figure 10**. A head-to-head summary of crop row extraction performance among the three methods is compiled in **Table 3**.

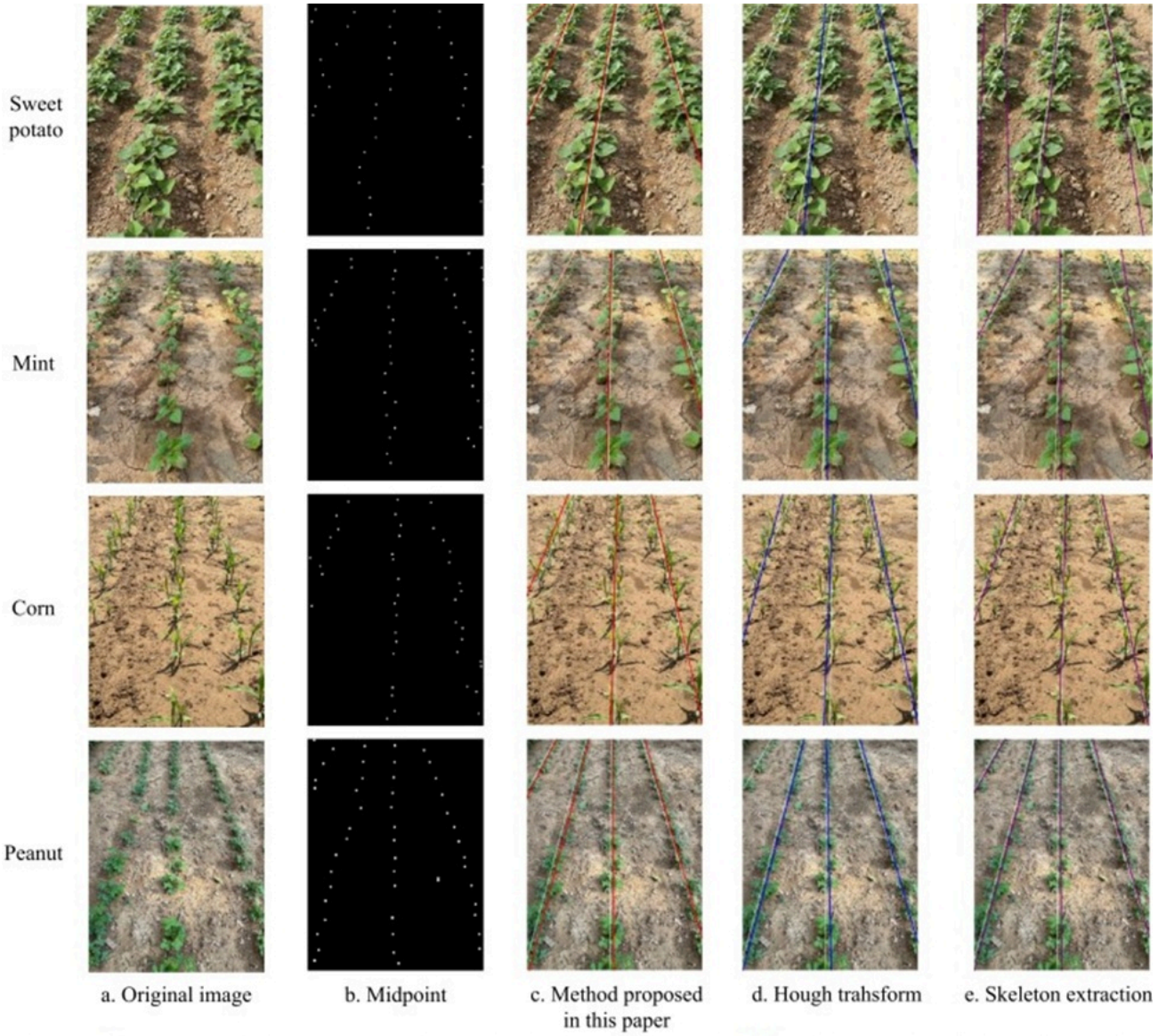

Note: In Fig. 10b, the midpoint image is obtained using the method proposed in this paper. Fig. 10c-10d show the crop row reference lines manually generated using a crop row annotation tool, where the white lines represent the manually generated reference lines, the red lines represent the crop row lines obtained using the method proposed in this paper, the blue lines represent the crop row lines obtained using the Hough transform method, and the purple lines represent the crop row lines obtained using the skeleton extraction method.

© 2022 The Author(s). | Published by Agro Intelligence Research Press

Figure 10. Experimental results comparison chart.

Table 3. Comparison of three detection methods of crop rows.

Crops	Detection methods	Mean processing time/ms	Mean error angle/(°)	Row recognition rate /(%)
Sweet potato	MS	91.83	0.76	100.00
	HF	183.65	6.60	66.67
	SE	295.21	14.05	91.66
Mint	MS	194.12	1.26	98.33
	HT	251.43	3.36	65.00
	SE	173.90	2.44	94.44
Corn	MS	83.16	1.05	100.00
	HT	189.72	3.31	80.00
	SE	179.54	3.61	95.56
Peanut	MS	175.45	0.72	95.00
	HT	196.65	1.15	71.42
	SE	245.21	0.76	95.00
Mean for all samples	MS	136.14	0.95	98.33
	HT	205.36	3.58	70.77
	SE	223.47	5.22	94.17

Note: MS designates the method of this paper, HT designates Hough Transform, and SE designates Skeleton extraction.

Throughout the crop row extraction evaluation, our methodology achieved a mean recognition score of 98.33% across all observable crop rows in 120 sample images from four field settings, outperforming both the Hough transform approach (70.77%) and the skeleton extraction approach (91.66%). Regarding sweet potato scenes, characterized by tight inter-row spacing and pervasive leaf intermingling due to rampant vegetative expansion, our strategy efficiently controls feature duration. It neutralizes the distorting effect of excess feature points by fusing adjoining crop structures into unified clusters and computing regional midpoints. The Hough transform alternative, in contrast, leans heavily on manual accumulator threshold calibration; it logged a per-image processing latency of 183.65 ms, a row recognition figure of 66.67%, and a mean angular deviation of 6.60°. The skeleton-based pipeline, constrained by the tangled skeleton profiles produced by the sweet potato's thick canopy, struggled to reliably extract centerlines, posting a row recognition figure of 91.66%, a mean angular deviation of 14.05°, and an individual image processing lag of 295.21 ms. Set against these benchmarks, our solution offers pronounced benefits: it successfully recovers every visible row in sweet potato imagery, even within the tightly bunched peripheral zones, achieving a perfect 100% row recognition figure alongside a minimal mean angular deviation of just 0.76°.

Switching to peppermint row extraction, our pipeline correctly identified all rows that could be adequately binarized, except for a handful near the image borders whose color signatures were too faint. For this crop, the skeleton extraction method achieved a recognition rate of 94.44%, but the wide morphological variability of peppermint foliage and persistent skeleton fragmentation constrained its performance. These shortcomings led to incorrect interpretation of skeleton cues in

© 2022 The Author(s). | Published by Agro Intelligence Research Press

zones of leaf overlap, causing the fitted centerlines to deviate from the actual row paths. At the same time, the Hough transform was affected by perspective foreshortening, which compressed and broke up crop rows, detecting only faint rows in the middle image region, yielding a recognition figure of merely 65.00% and a mean angular deviation substantially larger than our method's.

In the case of maize imagery, where missing plants and wide inter-plant spacing created row discontinuities in the binarized output, the skeleton extraction method achieved a recognition rate of 95.56%. Yet it failed to adequately bridge the skeleton terminals of detached plants, leading the empty inter-plant stretches to be misinterpreted as row terminations and fragmenting the centerlines. The Hough transform, by virtue of its rigid, linear detection paradigm, could not flexibly adapt to the needs of discontinuous row fitting, resulting in a mean angular deviation of 3.31° relative to the ground-truth row lines. Our method, by comparison, adaptively broadened the cluster search neighborhood to stitch discrete plants across gaps, constraining the mean angular deviation to 1.05° while still capturing every visible row throughout the tested scenarios.

Across the complete set of results, our research method consistently outperforms both the Hough transform and skeleton extraction pipelines in row recognition percentage, mean angular deviation, and mean processing time per image for the crop row extraction task. With an overall mean row recognition percentage of 98.33%, a mean angular deviation of 0.95°, and a markedly reduced per-image runtime of only 136.14 ms, our technique handily beats the Hough transform's average runtime of 205.36 ms. It delivers distinctly stronger performance than skeleton extraction across all metrics.

Error analysis of the experiment

In the centerline extraction trials conducted here, excessive spacing between consecutive plants within a row can affect how the DBSCAN algorithm forms clusters. As shown in **Figure 11**, some rows exhibit extremely wide gaps between adjacent plants. When DBSCAN runs, it determines whether sample points belong to the same cluster based on a user-specified distance cutoff. Under the conditions shown, the configured cutoff is set too conservatively, so the algorithm fails to link feature points arising from plants that, in truth, occupy the same row but are far apart. The red and blue clusters—which in reality correspond to a single crop row—are erroneously partitioned into separate classes because the interspace between them lies beyond the cutoff. This sorting mistake feeds directly into a duplicate line-fitting issue at later processing stages, so that the fitted trajectories fail to map accurately onto the genuine crop row centerlines, eroding both the correctness and the trustworthiness of the experimental findings and departing from the study's aim of reliably pinpointing crop row centerlines. As a next step, we plan to profile the spacing distributions characteristic of different crop rows statistically. By incorporating a machine learning module, the algorithm can self-tune and adapt its thresholds to the specific conditions of each scenario, thereby strengthening its resilience to variations in planting spacing.

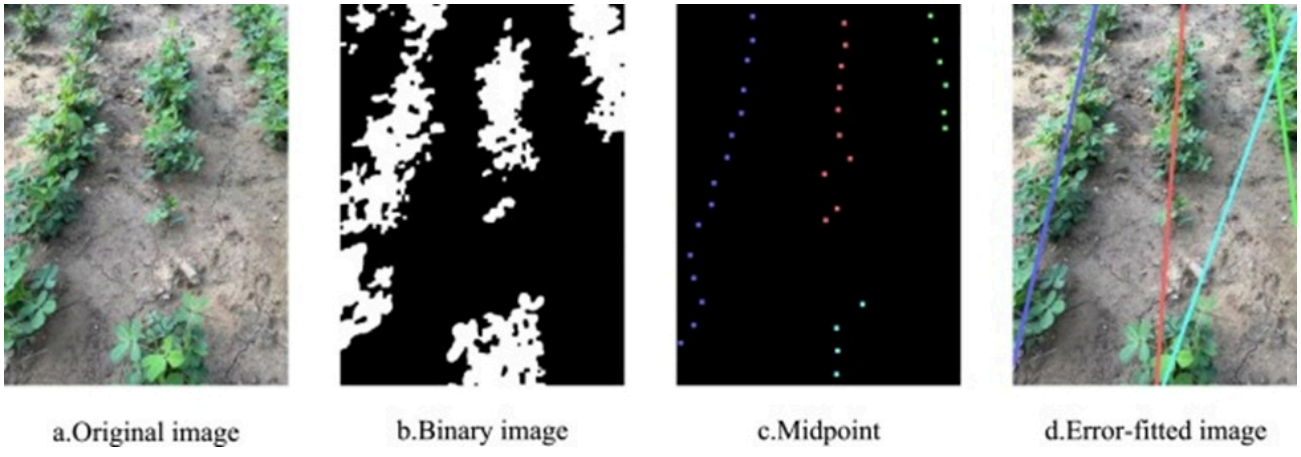

Figure 11. Experimental error analysis.

© 2022 The Author(s). | Published by Agro Intelligence Research Press

Conclusion

This study is motivated by the problem of insufficient accuracy and lengthy processing times in crop row extraction, arising from diverse crop types, heterogeneous growth environments, and inconsistent numbers of crop rows. We introduce a technique for extracting crop row centerlines that relies on region-based feature-point clustering. The procedure draws on the 2G-R-B grayscale transformation, along with median filtering and morphological operations, to suppress noise and weed-related disturbances. Through a series of preparatory image-processing trials, we have successfully mitigated the effects of variable illumination and weed intrusion, achieving reliable separation between green crops and the soil matrix.

We apply the Harris corner detector to extract feature points along crop rows and implement a region-based feature-point clustering scheme to consolidate crops, tag each row, and compute the row midpoint. This design mitigates interference from redundant feature points, boosting both the detection rate and the fidelity of crop-row identification while reducing the time overhead of image processing.

The algorithm presented here processes a typical 480 × 640 image in 136.14 ms. The centerline extraction approach built around region-based feature point clustering delivers a mean row recognition rate of 98.33% and a mean angular error of 0.95° across the four crop varieties examined. Its average accuracy advantage over the Hough transform is 2.63°, clearly demonstrating its substantial performance edge.

Acknowledgements

None

Conflict of interest

None

Financial support

None

Ethics statement

None

Received: 21 Jun 2021 Revised: 26 Aug 2021 Accepted: 10 Sep 2021
Published online: 25 May 2022

Rights and permissions

Open Access The author(s) retain copyright. This article is licensed under the Creative Commons Attribution-NonCommercial-ShareAlike 4.0 International License. It may be shared and adapted for non-commercial purposes with appropriate attribution, an indication of changes, and distribution of adaptations under the same license. Third-party material may be subject to separate terms identified in its credit line. View the license at https://creativecommons.org/licenses/by-nc-sa/4.0/.

References

1. Tang Y, Chen M, Wang C, Luo L, Li J, Lian G, et al. Recognition and localization methods for vision-based fruit picking robots: A review. Front Plant Sci. 2020;11:510.

2. Bai Y, Zhang B, Xu N, Zhou J, Shi J, Diao Z. Vision-based navigation and guidance for agricultural autonomous vehicles and robots: a review. Comput Electron Agric. 2023;205:107584.

3. Diao Z, Yan J, He Z, Zhao S, Guo P. Corn seedling recognition algorithm based on hyperspectral image and lightweight-3D-CNN. Comput Electron Agric. 2022;201:107343.

4. Chen J, Qiang H, Wu J, Xu G, Wang Z. Navigation path extraction for greenhouse cucumber-picking robots using the prediction-point Hough transform. Comput Electron Agric. 2021;180:105911.

5. Lu W, Zeng M, Wang L, Luo H, Mukherjee S, Huang X, et al. Navigation algorithm based on the boundary line of tillage soil combined with guided filtering and improved anti-noise morphology. Sensors. 2019;19(18):3918.

6. García-Santillán ID, Montalvo M, Guerrero JM, Pajares G. Automatic detection of curved and straight crop rows from images in maize fields. Biosyst Eng. 2017;156:61-79.

7. Diao Z, Guo P, Zhang B, Zhang D, Yan J, He Z, et al. Maize crop row recognition algorithm based on improved UNet network. Comput Electron Agric. 2023;210:107940.

8. Zhang Q, Chen MS, Li B. A visual navigation algorithm for paddy field weeding robot based on image understanding. Comput Electron Agric. 2017;143:66-78.

9. Midtiby HS, Åstrand B, Jørgensen O, Jørgensen RN. Upper limit for context-based crop classification in robotic weeding applications. Biosyst Eng. 2016;146:183-92.

10. Ball D, Upcroft B, Wyeth G, Corke P, English A, Ross P, et al. Vision-based obstacle detection and navigation for an agricultural robot. J Field Robot. 2016;33(8):1107-30.

11. Zhai Z, Zhu Z, Du Y, Song Z, Mao E. Multi-crop-row detection algorithm based on binocular vision. Biosyst Eng. 2016;150:89-103.

12. Ponnambalam VR, Bakken M, Moore RJ, Glenn Omholt Gjevestad J, From PJ. Autonomous crop row guidance using adaptive multi-ROI in strawberry fields. Sensors. 2020;20(18):5249.

13. Winterhalter W, Fleckenstein FV, Dornhege C, Burgard W. Crop row detection on tiny plants with the pattern hough transform. IEEE Robot Autom Lett. 2018;3(4):3394-401.

14. García-Santillán I, Guerrero JM, Montalvo M, Pajares G. Curved and straight crop row detection by accumulation of green pixels from images in maize fields. Precis Agric. 2018;19:18-41.

15. Jiang G, Wang X, Wang Z, Liu H. Wheat rows detection at the early growth stage based on Hough transform and vanishing point. Comput Electron Agric. 2016;123:211-23.

16. Zhang X, Li X, Zhang B, Zhou J, Tian G, Xiong Y, et al. Automated robust crop-row detection in maize fields based on position clustering algorithm and shortest path method. Comput Electron Agric. 2018;154:165-75.

17. Diao Z, Ma S, Zhang D, Zhang J, Guo P, He Z, et al. Algorithm for corn crop row recognition during different growth stages based on the ST-YOLOv8s network. Agronomy. 2024;14(7).

18. Vidović I, Cupec R, Hocenski Ž. Crop row detection by global energy minimization. Pattern Recognit. 2016;55:68-86.

© 2022 The Author(s). | Published by Agro Intelligence Research Press

19. Diao Z, Guo P, Zhang B, Zhang D, Yan J, He Z, et al. Navigation line extraction algorithm for corn spraying robot based on improved YOLOv8s network. Comput Electron Agric. 2023;212:108049.

20. Pang Y, Shi Y, Gao S, Jiang F, Veeranampalayam-Sivakumar A-N, Thompson L, et al. Improved crop row detection with deep neural network for early-season maize stand count in UAV imagery. Comput Electron Agric. 2020;178:105766.

21. Hamuda E, Glavin M, Jones E. A survey of image processing techniques for plant extraction and segmentation in the field. Comput Electron Agric. 2016;125:184-99.

22. Yin X, Du J, Noguchi N, Yang T, Jin C. Development of autonomous navigation system for rice transplanter. Int J Agric Biol Eng. 2018;11(6):89-94.

23. Ji B, Zhao J, Tao F, Zhang J, Zhang G, Wang N, et al. A novel nectarine fruit maturity detection and classification counting model based on YOLOv8n. IEEE Trans AgriFood Electron. 2025;3(1):144-55.

24. Ji B, Zhang J, Zhang H, Yu Y, Zhang G, Fan H, et al. Performance analysis of ris-enhanced secure transmission for symbiotic iov systems. IEEE Trans Cogn Commun Netw. 2025;11(1):454-64.

25. Ji B, Wang S, Chen H, Jin X, Zeng S, Song X, et al. Vehicular communication based on RIS-assisted source: RIS-relay versus energy harvesting relay. IEEE Trans Intell Transp Syst. 2024:1-20.

26. Wang W, Zhang X, Wei X. A review on weed detection using ground-based machine vision and image processing techniques. Comput Electron Agric. 2019;158:226-40.

27. Yang D, Li H, Liu S, Song C, Yang Y, Shen S, et al. In situ capture of spatter signature of SLM process using maximum entropy double threshold image processing method based on genetic algorithm. Opt Laser Technol. 2020;131:106371.

28. Ji B, Wang L, Tao F, Wang N, Zhang J, Zhang G, et al. Research on task offloading and delay optimization of unmanned aerial vehicle-assisted medical edge computing based on deep reinforcement learning. IEEE Trans Consum Electron. 2024:1-1.

29. Ji B, Li Y, Cao D, Li C, Mumtaz S, Wang D. Secrecy performance analysis of UAV assisted relay transmission for cognitive network with energy harvesting. IEEE Trans Veh Technol. 2020;69(7):7404-15.

30. Ji B, Li H, Jin X, Zhang J, Tao F, Li P, et al. Light-weight tomato leaf intelligent disease detection model based on adaptive kernel convolution and feature fusion. IEEE Trans AgriFood Electron. 2024;2(2):563-75.

31. Ji B, Sun K, Wang W, Li Y, Zhang J, Zhang G, et al. Relay cooperative vehicular communication system: RIS-equipped RF source with different types of forwarding method. IEEE Trans Intell Transp Syst. 2025:1-11.

© 2022 The Author(s). | Published by Agro Intelligence Research Press